Dynamical mean-field approximation to small-world networks of spiking neurons: From local to global and/or from regular to random couplings

Hideo Hasegawa*
Department of Physics, Tokyo Gakugei University, Koganei, Tokyo 184-8501, Japan
(Received 12 May 2004; published 3 December 2004)

By extending a dynamical mean-field approximation previously proposed by the author [H. Hasegawa, Phys. Rev. E **67**, 041903 (2003)], we have developed a semianalytical theory which takes into account a wide range of couplings in a small-world network. Our network consists of noisy N-unit FitzHugh-Nagumo neurons with couplings whose average coordination number Z may change from local ($Z \ll N$) to global couplings ($Z=N-1$) and/or whose concentration of random couplings p is allowed to vary from regular ($p=0$) to completely random ($p=1$). We have taken into account three kinds of spatial correlations: the on-site correlation, the correlation for a coupled pair, and that for a pair without direct couplings. The original $2N$-dimensional *stochastic* differential equations are transformed to 13-dimensional *deterministic* differential equations expressed in terms of means, variances, and covariances of state variables. The synchronization ratio and the firing-time precision for an applied single spike have been discussed as functions of Z and p. Our calculations have shown that with increasing p, the synchronization is *worse* because of increased heterogeneous couplings, although the average network distance becomes shorter. Results calculated by our theory are in good agreement with those by direct simulations.

DOI: 10.1103/PhysRevE.70.066107 PACS number(s): 05.45.−a, 84.35.+i, 87.10.+e, 07.05.Mh

I. INTRODUCTION

It is well known that a brain forms complex networks with nodes (neurons) and links (axons and dendrites). A small patch of cortex may contain thousands of similar neurons, each connecting with hundreds or thousands of other neurons in that same patch or in other patches through axons and dendrites. The underlying dynamics of individual neurons is described by Hodgkin-Huxley-type nonlinear differential equations (DE's). Many theoretical studies have been reported on dynamics of large-scale neuron networks. Extensive numerical calculations have been made by using various spiking neuron models such as Hodgkin-Huxley (HH) [1], FitzHugh-Nagumo (FN) [2,3], and Hindmarsh-Rose (HR) models [4]. These theoretical studies have been performed with the use of the two approaches: direct simulations and analytical methods such as the Fokker-Planck equation [5], the population density method [6,7], and the moment method [8–11]. Since the computation time of direct simulations is proportional to N^2, simulations for actual network size become difficult, where N is the size of a given neuron network. The Fokker-Planck equation method is mainly applied to $N=\infty$ network with the mean-field and/or diffusion approximations [12]. The population method has been employed for a large-scale integrate-and-fire (IF) neuron network [6,7]. The moment method has been applied to FN and HH neuron models [8–11].

Most of theoretical studies have assumed that couplings in neuron networks are local ($Z \ll N$) or global ($Z=N-1$), and/or regular ($p=0$) or random ($p=1$), where Z and p denotes the average coordination number and the concentration of random couplings, respectively. In real neuron networks, however, couplings are neither local nor global with the degree of randomness locating between the two extremes of regular and random couplings. In recent years, much attention has been paid to *small-world* (SW) networks with the finite degree of heterogeneity in couplings, which is characterized by the high clustering and the small average distance between nodes [13–16]. The SW property is realized in various kinds of biological, social, and technological systems such as the electric power grid, the movie-star collaborations, and the neuronal network of the nematode worm *C. elegans* [13,14]. Some calculations have been reported for neural networks of spiking neuron models as well as of phase models [17–23]. It has been shown that by introducing the coupling heterogeneity into SW networks, the synchronization is *increased* because the average distance in SW networks is shorter than that in regular networks [17–19,21–23]. Recently, however, Nishikawa *et al.* [20] have claimed that the synchronization is *decreased* with including the coupling heterogeneity in SW networks. Then it has been controversial whether the synchronization in SW networks is better or worse than in regular networks. These studies on SW networks have entirely relied on direct simulations, and it is desirable to make a study by using an analytical method.

In the previous papers of Refs. [24] and [25] (which are referred to as I and II), the present author proposed a semianalytical dynamical mean-field approximation (DMA) theory for a study on neuron ensembles (networks) with all-to-all (global) couplings. In I, DMA was applied to an N-unit FN neuron network, for which $2N$-dimensional stochastic DE's are transformed to eight-dimensional deterministic DE's expressed by means, variances, and covariances of state variables. In the subsequent II, DMA was applied to networks consisting of general spiking neurons, each of which is described by M variables. MN-dimensional stochastic DE's are transformed to N_{eq} deterministic DE's where N_{eq}

*Email address: hasegawa@u-gakugei.ac.jp

$=M(M+2)$. The DMA theory was successfully applied to a HH neuron network with $N_{eq}=24$ in II. Advantages of DMA are (1) some qualitative properties of networks are derived without numerical computations, and (2) the computational time of DMA is much shorter than those of the moment method [26] and direct simulations. As for the item (2), for example, the former is thousands of times faster than the latter for $N=100$ HH neuron network with 100 trials [25].

The purpose of the present paper is to develop a semianalytical approach for SW neural networks of FN neurons with general couplings, extending our DMA [24,25]. In I and II, interactions among neurons are assumed to be all-to-all (global) couplings. For DMA to include local couplings in SW networks, we have taken into account variances and covariances which express three kinds of spatial correlations: (i) on-site correlation, (ii) the correlation for a coupled pair, and (iii) that for an uncoupled pair without direct couplings. Assuming that the heterogeneity is small, we have included its effects in order to discuss the synchronization in SW networks.

The paper is organized as follows. In Sec. II, we have derived DE's, applying the DMA to SW networks consisting of FN neurons which are coupled with the average coordination number Z. The original $2N$-dimensional stochastic DE's are transformed to 13-dimensional deterministic DE's. In Sec. III A, we report numerical calculations for regular networks by changing Z from local ($Z \ll N$) to global couplings ($Z=N-1$). The Z dependence of the firing-time accuracy and the synchronization ratio for an applied single spike is discussed. Numerical calculations for SW networks are reported in Sec. III B, where the effect of the concentration of random couplings is discussed. The final Sec. IV is devoted to conclusion and discussion.

II. SMALL-WORLD NETWORKS OF FN NEURONS

A. Adopted model and method

We have assumed that N-unit FN neurons are distributed on a ring with the average coordination number Z and the concentration of random couplings p. Dynamics of a single neuron i in a given SW network is described by the nonlinear DE's given by

$$\frac{dx_{1i}(t)}{dt} = F[x_{1i}(t)] - cx_{2i}(t) + I_i^{(c)}(t) + I_i^{(e)}(t) + \xi_i(t), \quad (1)$$

$$\frac{dx_{2i}(t)}{dt} = bx_{1i}(t) - dx_{2i}(t) + e, \quad (i = 1 \text{ to } N) \quad (2)$$

with

$$I_i^{(c)}(t) = J\sum_j c_{ij} G(x_{1j}(t)), \quad (3)$$

$$I_i^{(e)}(t) = A\Theta(t - t_{in})\Theta(t_{in} + t_w - t). \quad (4)$$

In Eqs. (1)–(4), $F[x(t)]=kx(t)[x(t)-a][1-x(t)]$, $k=0.5$, $a=0.1$, $b=0.015$, $d=0.003$, and $e=0$ [8,9,24]: x_{1i} and x_{2i} denote the fast (voltage) variable and slow (recovery) variable, respectively: $G(x)$ stands for the sigmoid function given by $G(x)=1/\{1+\exp[-(x-\theta)/\alpha]\}$ with threshold θ and width α: J the coupling strength: c_{ij} the coupling matrix given by $c_{ij}=c_{ji}=1$ for a coupled (i,j) pair and zero otherwise, self-coupling terms being excluded ($c_{ii}=0$). By changing Z value, our model given by Eqs. (1)–(4) covers from local couplings ($Z \ll N$) to global couplings ($Z=N-1$). We have studied the response of neuron networks to an external, single spike input given by $I_i^{(e)}(t)$ with magnitude A and spike width t_w applied at the input time t_{in}, $\Theta(x)$ being the Heaviside function. Added white noises $\xi_i(t)$ are given by

$$\langle \xi_i(t) \rangle = 0, \quad (5)$$

$$\langle \xi_i(t)\xi_j(t') \rangle = \beta^2 \delta_{ij}\delta(t - t'), \quad (6)$$

where the average of $\langle U(\mathbf{z},t) \rangle$ for an arbitrary function of $U(\mathbf{z},t)$ is given by

$$\langle U(\mathbf{z},t) \rangle = \int \cdots \int d\mathbf{z} U(\mathbf{z},t) \Pr(\mathbf{z}), \quad (7)$$

$\Pr(\mathbf{z})$ denoting a probability distribution function for $2N$-dimensional random variables $\mathbf{z}=(\{x_{\kappa i}\})$.

An SW network is made after the Watts-Strogatz model [13]. Starting from the regular coupling for which $c_{ij} \equiv c_{0ij}$, N_{ch} couplings among $NZ/2$ couplings are randomly modified such that $c_{0ij}=0$ is changed to $c_{ij}=1$ or vice versa. The concentration of random couplings is given by

$$p = \frac{2N_{ch}}{NZ}, \quad (8)$$

which is 0 and 1 for completely regular and random couplings, respectively. We shall take into account the effect of the heterogeneity given by

$$\frac{\delta c_{ij}}{Z} = \frac{1}{Z}(c_{ij} - c_{0ij}), \quad (9)$$

assuming it is small.

After I, we will obtain equations of motions for means, variances, and covariances of state variables. Variables spatially averaged over the ensemble are defined by

$$X_\kappa(t) = \frac{1}{N}\sum_i x_{\kappa i}, \quad \kappa = 1,2 \quad (10)$$

and their means by

$$\mu_\kappa(t) = \langle\langle X_\kappa(t) \rangle\rangle_c, \quad (11)$$

where the bracket $\langle\cdot\rangle_c$ denotes the average over the coupling configuration. As for variances and covariances of state variables, we consider three kinds of spatial correlations: (i) on-site correlation (γ), (ii) the correlation for a coupled pair (ζ) and (iii) that for a pair without direct couplings (η):

$$\langle\langle \delta x_{\kappa i}\delta x_{\lambda j} \rangle\rangle_c = \begin{cases} \gamma_{\kappa,\lambda}, & \text{for } i = j \\ \zeta_{\kappa,\lambda}, & \text{for } i \neq j, c_{ij} = 1 \\ \eta_{\kappa,\lambda}, & \text{for } i \neq j, c_{ij} = 0, \end{cases} \quad (12)$$

where $\kappa,\lambda=1,2$ and

$$\delta x_{\kappa i}(t) = x_{\kappa i}(t) - \mu_\kappa(t). \tag{13}$$

In Eq. (12) , $\gamma_{\kappa,\lambda}$, $\zeta_{\kappa,\lambda}$ and $\eta_{\kappa,\lambda}$ are defined by

$$\gamma_{\kappa,\lambda}(t) = \left\langle \frac{1}{N}\sum_i \langle \delta x_{\kappa i}(t)\, \delta x_{\lambda i}(t)\rangle \right\rangle_c, \tag{14}$$

$$\zeta_{\kappa,\lambda}(t) = \left\langle \frac{1}{NZ}\sum_i \sum_j c_{ij}\langle \delta x_{\kappa i}(t)\, \delta x_{\lambda j}(t)\rangle \right\rangle_c, \tag{15}$$

$$\eta_{\kappa,\lambda}(t) = \left\langle \frac{1}{N(N-Z-1)}\sum_i \sum_j (1-\delta_{ij}-c_{ij})\langle \delta x_{\kappa i}(t)\, \delta x_{\lambda j}(t)\rangle \right\rangle_c. \tag{16}$$

For a later purpose, we also define the spatially averaged correlation given by

$$\rho_{\kappa,\lambda}(t) = \left\langle \frac{1}{N^2}\sum_i \sum_j \langle \delta x_{\kappa i}(t)\, \delta x_{\lambda j}(t)\rangle \right\rangle_c, \tag{17}$$

$$= \langle\langle \delta X_\kappa(t)\, \delta X_\lambda(t)\rangle\rangle_c, \tag{18}$$

where $\delta X_\kappa(t) = X_\kappa(t) - \mu_\kappa(t)$. It is noted that $\gamma_{\kappa,\lambda}$, $\zeta_{\kappa,\lambda}$, $\eta_{\kappa,\lambda}$, and $\rho_{\kappa,\lambda}$ are not independent, obeying the sum rule given by

$$N\rho_{\kappa,\lambda} = \gamma_{\kappa,\lambda} + Z\zeta_{\kappa,\lambda} + (N-Z-1)\,\eta_{\kappa,\lambda}. \tag{19}$$

In order to derive Eqs. (14)–(19), we have employed the decomposition

$$1 = \delta_{ij} + (1-\delta_{ij})[c_{ij} + (1-c_{ij})] = \delta_{ij} + c_{ij} + (1-\delta_{ij}-c_{ij}), \tag{20}$$

with $c_{ii} = 0$.

In calculating means, variances, and covariances given by Eqs. (11) and (14)–(19), we have assumed that (i) the noise intensity is weak, (ii) the distribution of state variables takes the Gaussian form, and (iii) the coupling heterogeneity of $\delta c_{ij}/Z$ is small. By using the first assumption, we expand DE's given by Eqs. (1)–(4) in a power series of fluctuations around means. The second assumption may be justified by some numerical calculations for FN [9,27] and HH neuron models [28,29]. Based on the third assumption, the effect of coupling fluctuations has been taken into account up to the order of $O((\delta c_{ij}/Z)^2)$.

Before closing Sec. II A, we briefly summarize the introduced variables and their meanings as follows: N, the number of neurons: Z, the average coordination number: p, the concentration of random couplings: J, the coupling strength: c_{ij}, the coupling matrix between neurons i and j: X_κ, the spatially average of the fast ($\kappa=1$) and slow ($\kappa=2$) variables; μ_κ, a mean value of X_κ; $\gamma_{\kappa,\lambda}$, $\zeta_{\kappa,\lambda}$, and $\eta_{\kappa,\lambda}$, the correlations of on-site, a coupled pair, and an uncoupled pair, respectively. Readers who are not interested in mathematical details, may skip to Sec. II C where a summary of our method is presented.

B. Equations of motions

After some manipulations, we get the following DE's (the argument t being suppressed; for details, see the Appendix):

$$\frac{d\mu_1}{dt} = f_0 + f_2\gamma_{1,1} - c\mu_2 + JZ(g_0 + g_1\phi_1) + I_{ext}, \tag{21}$$

$$\frac{d\mu_2}{dt} = b\mu_1 - d\mu_2 + e, \tag{22}$$

$$\frac{d\gamma_{1,1}}{dt} = 2(a\gamma_{1,1} - c\gamma_{1,2}) + 2JZ(g_1\zeta_{1,1} + g_0\phi_1) + \beta^2, \tag{23}$$

$$\frac{d\gamma_{2,2}}{dt} = 2(b\gamma_{1,2} - d\gamma_{2,2}), \tag{24}$$

$$\frac{d\gamma_{1,2}}{dt} = b\gamma_{1,1} + (a-d)\gamma_{1,2} - c\gamma_{2,2} + JZ(g_1\zeta_{1,2} + g_0\phi_2), \tag{25}$$

$$\frac{d\rho_{1,1}}{dt} = 2(a\rho_{1,1} - c\rho_{1,2}) + \left(\frac{2JZg_1}{N}\right) \times[\gamma_{1,1} + ZR\zeta_{1,1} + (N-ZR-1)\,\eta_{1,1}] + \frac{\beta^2}{N}, \tag{26}$$

$$\frac{d\rho_{2,2}}{dt} = 2(b\rho_{1,2} - d\rho_{2,2}), \tag{27}$$

$$\frac{d\rho_{1,2}}{dt} = b\rho_{1,1} + (a-d)\rho_{1,2} - c\rho_{2,2} + \left(\frac{JZg_1}{N}\right) \times[\gamma_{1,2} + ZR\zeta_{1,2} + (N-ZR-1)\,\eta_{1,2}], \tag{28}$$

$$\frac{d\zeta_{1,1}}{dt} = 2(a\zeta_{1,1} - c\zeta_{1,2}) + 2Jg_1 \times[\gamma_{1,1} + ZC\zeta_{1,1} + (ZR-ZC-1)\,\eta_{1,1}], \tag{29}$$

$$\frac{d\zeta_{2,2}}{dt} = 2(b\zeta_{1,2} - d\zeta_{2,2}), \tag{30}$$

$$\frac{d\zeta_{1,2}}{dt} = b\zeta_{1,1} + (a-d)\zeta_{1,2} - c\zeta_{2,2} + Jg_1 \times[\gamma_{1,2} + ZC\zeta_{1,2} + (ZR-ZC-1)\,\eta_{1,2}], \tag{31}$$

$$\frac{d\eta_{1,1}}{dt} = 2(a\eta_{1,1} - c\eta_{1,2}) + \left(\frac{2JZg_1}{N-Z-1}\right)\{g_1[(ZR-ZC-1)\zeta_{1,1} + (N-2ZR+ZC)\,\eta_{1,1}] - g_0\phi_1\}, \tag{32}$$

$$\frac{d\eta_{2,2}}{dt} = 2(b\eta_{1,2} - d\eta_{2,2}), \tag{33}$$

$$\frac{d\eta_{1,2}}{dt} = b\eta_{1,1} + (a-d)\eta_{1,2} - c\eta_{2,2} + \left(\frac{JZ}{N-Z-1}\right) \times \{g_1[(ZR - ZC - 1)\zeta_{1,2} + (N - 2ZR + ZC)\eta_{1,2}] - g_0\phi_2\}, \tag{34}$$

$$\frac{d\phi_1}{dt} = a\phi_1 - c\phi_2 + JZg_0\delta R_p, \tag{35}$$

$$\frac{d\phi_2}{dt} = b\phi_1 - d\phi_2, \tag{36}$$

with

$$\phi_\kappa(t) = \left\langle \frac{1}{NZ}\sum_i \sum_j \langle \delta x_i \delta c_{ij} \rangle \right\rangle_c, \quad \kappa = 1,2, \tag{37}$$

$$C = \frac{1}{NZ^2}\sum_i \sum_j \sum_k c_{0ij}c_{0jk}c_{0ik}, \tag{38}$$

$$R = \frac{1}{NZ^2}\sum_i \sum_j \sum_k c_{0ij}c_{0jk}, \tag{39}$$

$$\delta R_p = \left\langle \frac{1}{NZ^2}\sum_i \sum_j \sum_k \delta c_{ij}\delta c_{jk} \right\rangle_c, \tag{40}$$

where $a = f_1 + 3f_3\gamma_{1,1}$, $f_\ell = (1/\ell!)F^{(\ell)}$, $g_\ell = (1/\ell!)G^{(\ell)}$, C corresponds to the clustering coefficient introduced in SW networks [13,14], R expresses the coupling connectivity, and δR_p is its fluctuation part, related discussions being given in Sec. IV.

C. Summary of our method

Equations of motions for $\mu_\kappa(t)$, $\gamma_{\kappa,\lambda}(t)$, $\zeta_{\kappa,\lambda}(t)$, $\eta_{\kappa,\lambda}(t)$, and $\rho_{\kappa,\lambda}(t)$ are given by Eqs. (21)–(40). In Eqs. (35) and (36), $\phi_\kappa(t)$ ($\kappa = 1,2$) are new correlation functions which appear in the process of calculating equations of motion of $\gamma_{\kappa,\lambda}$, etc. The factors C, R, and δR_p defined by Eqs. (38)–(40) generally depend on the geometry of a given neuron network. For a regular ring with even Z, we get $R=1$ and C given by

$$C = \begin{cases} 0, & \text{for } Z \leqslant 2 \\ 3/4 - 3/2Z, & \text{for } 4 \leqslant Z < 2N/3 \\ 3/4 - 3/2Z + 9/4 - (3N - 9/2)/Z + (N^2 - 3N + 2)/Z^2, & \text{for } 2N/3 \leqslant Z < N-1 \\ (1 - 1/Z) & \text{for } Z = N-1. \end{cases} \tag{41}$$

Figure 1 shows C as a function of Z/N for $N=100$, 200, 500, and 1000. We note that $C \sim 0.75$ for $0.1 < Z/N < 0.7$ and that $C \to (1-1/Z)$ as $Z/N \to (1-1/N)$. In the case of global couplings ($Z=N-1$), however, we get $C=(1-1/Z)$ independent of the geometry. δR_p defined by Eq. (40), which expresses fluctuations in heterogeneous couplings, is increased with increasing the concentration of random couplings, p [Fig. 6(a)]. Among the 12 correlations such as $\gamma_{\kappa,\lambda}$, etc., given by Eqs. (14)–(17), nine correlations are independent because of the sum rule given by Eq. (20). In this study, we have chosen nine correlations of $\gamma_{\kappa,\lambda}$, $\zeta_{\kappa,\lambda}$, and $\rho_{\kappa,\lambda}$ as independent variables. Then the original $2N$-dimensional *stochastic* DE's given by Eqs. (1) and (2) have been transformed to 13-dimensional *deterministic* DE's.

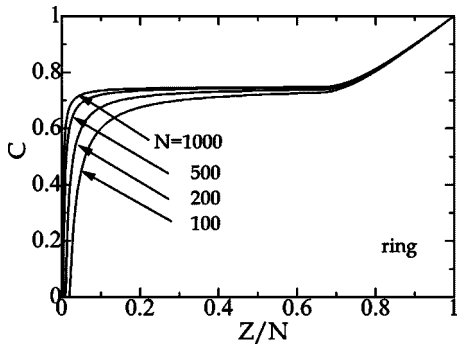

FIG. 1. The clustering coefficient C for a ring with regular couplings ($p=0$) as a function of Z/N for $N=100$, 200, 500, and 1000.

It is worthwhile to explain the relation between the present theory and I, where the original $2N$-dimensional stochastic DE's for regular, global couplings are transformed to eight-dimensional deterministic DE's. In the present study for the general coupling, we have to take into account $\zeta_{\kappa,\lambda}$ and $\eta_{\kappa,\lambda}$, in order to discriminate correlations between a coupled pair and an uncoupled pair. However, in the limit of $Z=N-1$ for regular, global couplings for which $R=1$ and $ZC=Z-1$, $\eta_{\kappa,\lambda}$ are not necessary because there are no uncoupled pairs: prefactors of $(ZR-ZC-1)$ for $\eta_{\kappa,\lambda}$ in Eqs. (32) and (34) vanish with $\phi_\kappa=0$. Then the number of required DE's is reduced from 13 to 8. Equations (21)–(28) for μ_κ, $\gamma_{\kappa,\lambda}$, and $\rho_{\kappa,\lambda}$ agree with Eqs. (20)–(27) in I [30].

D. Firing-time accuracy and synchronization

1. Firing-time accuracy

When we solve DE's given by Eqs. (21)–(36), we may obtain various quantities relevant to firings in neuron net-

works. The firing time of a given neuron i is defined as the time when the variable $x_{1i}(t)$ crosses the threshold θ from below:

$$t_{o\ell} = \{t | x_{1i}(t) = \theta; \dot{x}_i(t) > 0\}. \tag{42}$$

It has been shown that the distribution of firing times of $t_{o\ell}$ is given by [24]

$$Z_\ell(t) \sim \Phi\left(\frac{t - t_f}{\delta t_{o\ell}}\right) \frac{d}{dt}\left(\frac{\mu_1}{\sqrt{\gamma_{1,1}(t_f)}}\right) \Theta(\dot{\mu}_1), \tag{43}$$

$$\rightarrow \delta(t - t_f), \quad \text{for } \gamma_{1,1}(t_f) \rightarrow 0$$

with

$$\delta t_{o\ell} = \frac{\sqrt{\gamma_{1,1}(t_f)}}{\dot{\mu}_1}, \tag{44}$$

where Φ expresses the normal distribution function, the average firing time t_f is implicitly defined by $\mu_1(t_f) = \theta$, $\dot{\mu}_1 = \dot{\mu}_1(t_f)$ and the dot denotes the time derivative.

Similarly, the firing time of an averaged variable $X_1(t)$ is defined as the time when the variable $X_1(t)$ crosses the threshold θ from below:

$$t_{og} = \{t | X_1(t) = \theta; \dot{X}_1(t) > 0\}. \tag{45}$$

The distribution of firing times of t_{og} is given by [24]

$$Z_g(t) \sim \Phi\left(\frac{t - t_f}{\delta t_{og}}\right) \frac{d}{dt}\left(\frac{\mu_1}{\sqrt{\rho_{1,1}(t_f)}}\right) \Theta(\dot{\mu}_1), \tag{46}$$

$$\rightarrow \delta(t - t_f) \quad \text{for } \rho_{1,1}(t_f) \rightarrow 0$$

with

$$\delta t_{og} = \frac{\sqrt{\rho_{1,1}(t_f)}}{\dot{\mu}_1}. \tag{47}$$

2. Synchronization ratio

We discuss the synchronization in neuron networks, considering the quantity given by

$$R_s(t) = \frac{1}{N^2} \sum_i \sum_j \langle [x_i(t) - x_j(t)]^2 \rangle, \tag{48}$$

$$= 2(\gamma_{1,1} - \rho_{1,1}), \tag{49}$$

which vanishes in the completely synchronous state. From a comparison of Eqs. (23)–(25) with Eqs. (26)–(28), we note that

$$\rho_{\kappa,\lambda} = \frac{\gamma_{\kappa,\lambda}}{N}, \quad \text{for } J \rightarrow 0. \tag{50}$$

Then, $R_s(t)$ given by Eq. (49) becomes $R_s(t) = (1 - 1/N)\gamma_{1,1}(t) \equiv R_{s0}(t)$ in the asynchronous state, while $R_s(t) = 0$ in the completely synchronous state. We define the *synchronization ratio* at the firing time t_f by [24]

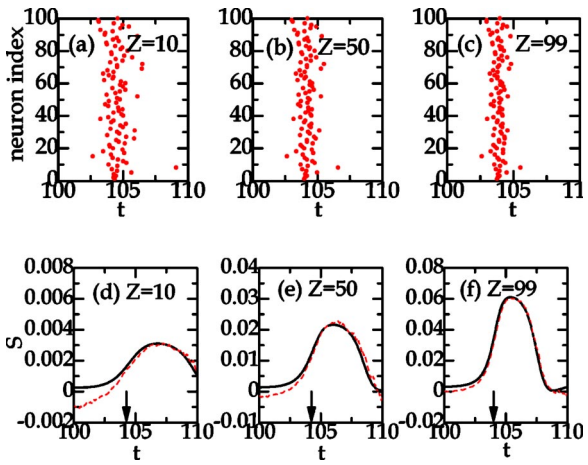

FIG. 2. (Color online) The plots showing firings in a regular neuron network for Z= (a) 10, (b) 50, and (c) 99 calculated by direct simulations (single trials), and time courses of $S(t)$ for Z= (d) 10, (e) 50, and (f) 99 calculated by DMA (solid curves) and direct simulations (dashed curves) (β=0.01, J=0.002, N=100, and p=0.0). Arrows in (d)–(f) denote firing times.

$$S_f = S(t_f), \tag{51}$$

with

$$S(t) = 1 - \frac{R_s(t)}{R_{s0}(t)} = \left(\frac{N\rho_{1,1}(t)/\gamma_{1,1}(t) - 1}{N - 1}\right), \tag{52}$$

which is 0 and 1 for completely asynchronous and synchronous states, respectively. The synchronization ratio shows much variety depending on model parameters such as the coupling strength (J), the noise intensity (β), the size of cluster (N), the coordination number (Z), and the random concentration (p), as will be discussed in Sec. III.

III. CALCULATED RESULTS

A. Regular couplings

We have adopted same parameters of θ=0.5, α=0.5, τ_s=10, A=0.10, t_{in}=100, and T_w=10 as in I [24]. DMA calculations have been made by solving Eqs. (21)–(36) with the use of the fourth-order Runge-Kutta method with the time step of 0.01. We have performed direct simulations by using also the fourth-order Runge-Kutta method with the time step of 0.01. Results of direct simulations are averages of 1000 trials for $Z \leqslant 20$ (or $N \leqslant 20$) and those of 100 trials otherwise noticed. All quantities are dimensionless.

First we discuss the case of regular couplings (p=0), by changing the average coordination number Z from local ($Z \ll N$) to global couplings ($Z = N - 1$). The plots in Figs. 2(a)–2(c) show firings in an N=100 neuron network with regular couplings for Z=10, 50, and 99 with β=0.01 and J=0.002 when a single external spike given by Eq. (4) is applied. Figures 2(a)–2(c) show that as increasing Z, scattering of firing times is reduced, which suggests an increase in the firing accuracy and the synchronization. These are results of direct simulations with single trials. They are more clearly discussed with calculations using the DMA.

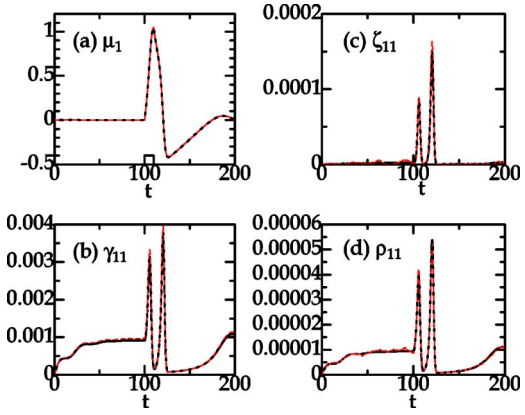

FIG. 3. (Color online) Time courses of (a) μ_1, (b) $\gamma_{1,1}$, (c) $\zeta_{1,1}$, and (d) $\rho_{1,1}$ for $\beta=0.01$, $J=0.002$, $N=100$, $Z=10$, and $p=0$, solid and dashed curves denoting results of DMA and direct simulations, respectively. At the bottom of (a), an input signal is plotted.

Figures 2(d)–2(f) show time courses of $S(t)$ calculated in the DMA for $Z=10$, 50, and 99, whose magnitudes are increased as increasing Z; note differences of the ordinate scales in Figs. 2(d)–2(f). The synchronization ratio at firing times, S_f, is 0.0019, 0.0113, and 0.0295 for $Z=10$, 50, and 99, respectively, which shows an increased synchrony with increasing Z.

We will discuss some details of the DMA calculation in Figs. 3(a)–3(d) which show time courses of μ_1, $\gamma_{1,1}$, $\zeta_{1,1}$, and $\rho_{1,1}$, respectively, for regular couplings ($p=0$) with $\beta=0.01$, $J=0.002$, $N=100$, and $Z=10$. Results of DMA expressed by solid curves are in good agreement with those of direct simulations depicted by dashed curves. Time courses of μ_1, $\gamma_{1,1}$, and $\rho_{1,1}$ shown in Figs. 3(a)–3(d) for local couplings ($Z=10$) are not so different from those for global couplings having been reported in Fig. 1 of I, except for their magnitudes. For example, DMA calculations for the local coupling with $Z=10$ in the case of $\beta=0.01$, $J=0.002$, and $N=100$ show that magnitudes of $\gamma_{1,1}$, $\zeta_{1,1}$, and $\rho_{1,1}$ at the firing time of $t=104.44$ are 0.271×10^{-2}, 0.475×10^{-4}, and 0.320×10^{-4}, respectively. In contrast, for the global coupling with $Z=99$, magnitudes of $\gamma_{1,1}$, $\zeta_{1,1}$, and $\rho_{1,1}$ at the firing time of $t=103.88$ are 0.235×10^{-2}, 0.693×10^{-4}, and 0.921×10^{-4}, respectively.

Figure 4(a) shows the Z dependence of $\gamma_{1,1}$, $\zeta_{1,1}$, and $\rho_{1,1}$ at the firing time with $J=0.002$, $\beta=0.01$, and $N=100$; filled and open marks express results of DMA and direct simulations, respectively. Results of $\gamma_{1,1}$ and $\rho_{1,1}$ of DMA are indistinguishable from those of direct simulations. With increasing Z, both $\zeta_{1,1}$ and $\rho_{1,1}$ are increased, while $\gamma_{1,1}$ is slightly decreased, as mentioned above. The Z dependence of the firing time t_f is plotted in Fig. 4(b), which shows the faster response for larger Z. This is due to the fact that by an increased Z, μ_1 is increased more rapidly to cross the threshold level of θ. Then $\dot{\mu}_1$ at $t=t_f$ is increased with increasing Z, as the chain curve in Fig. 4(c) shows. Figure 4(c) shows that with increasing Z, the firing-time accuracy of $\delta t_{o\ell}$ is improved while that of δt_{og} is independent of Z. The Z dependence of the synchronization is plotted in Fig. 4(d) showing S_f to be linearly increased for a small Z. This clearly explains

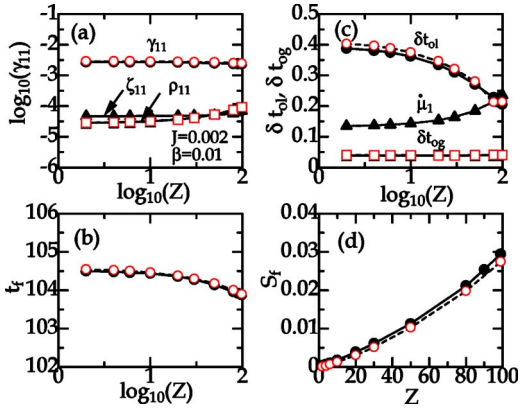

FIG. 4. (Color online) The Z dependence of (a) the correlations of $\gamma_{1,1}$ (circles), $\zeta_{1,1}$ (triangles), and $\rho_{1,1}$ (squares) at the firing time, (b) the firing times t_f, (c) the firing-time accuracy of $\delta t_{o\ell}$ (circles), δt_{og} (squares), and $\dot{\mu}_1$ (triangles), and (d) the synchronization ratio at the firing time, S_f, for $\beta=0.01$, $J=0.002$, and $N=100$: filled and open marks denote results of DMA and direct simulations, respectively. Results of $\zeta_{1,1}$ and $\dot{\mu}_1$ are only for DMA.

the larger synchrony S_f for larger Z, having been shown in Figs. 2(a)–2(f).

B. SW couplings

Next we discuss the case of SW couplings, by changing the concentration of random couplings p. The plots in Figs. 5(a)–5(c) show firings in SW networks for $p=0.0$, 0.1, and 1.0, respectively, with $\beta=0.005$ $J=0.02$, $N=100$, and $Z=10$ calculated by direct simulations with single trials, when a single external spike given by Eq. (4) is applied. In this subsection, we have adopted a smaller β and a larger J than in Sec. III A to get more evident effects of p. Figures 5(a)–5(c) show that as increasing p, scattering of firing times is gradually increased, which suggests a decrease in the firing-time accuracy and the synchronization. These results

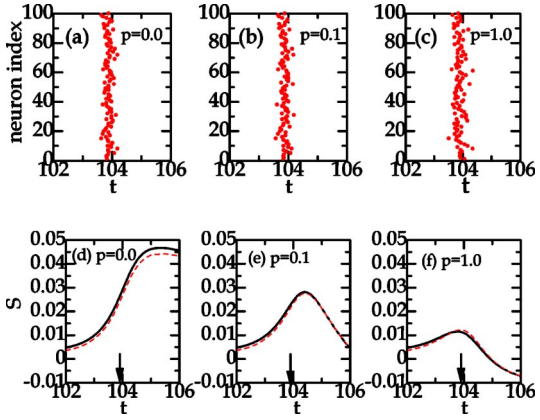

FIG. 5. (Color online) The plots showing firings in a small-world neuron network for $p=$ (a) 0.0, (b) 0.1, and (c) 1.0 calculated by direct simulations (single trials), and time courses of $S(t)$ for $p=$ (d) 0.0, (e) 0.1, and (f) 1.0 calculated by DMA (solid curves) and direct simulations (dashed curves) ($\beta=0.005$, $J=0.02$, $z=10$, and $N=100$). Arrows in (d)–(f) denote firing times.

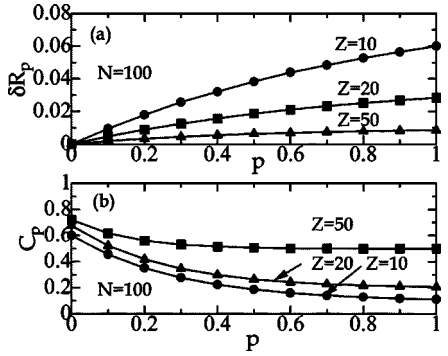

FIG. 6. The p dependence of (a) the factor δR_p and (b) the clustering coefficient C_p, for $Z=10$, 20, and 50 with $N=100$.

are more clearly seen in calculations with the use of DMA. Figures 5(d)–5(f) show time courses of $S(t)$ for $p=0$, 0.1, and 1.0, calculated in the DMA. The synchronization ratio at firing times S_f is 0.0256, 0.0224, and 0.0114, for $p=0$, 0.1, and 1.0, respectively. Although S_f for $p=0.1$ is nearly equal to that for $p=0.0$, the time course of $S(t)$ for $p=0.1$ is rather different from that for $p=0.0$.

This decrease in S_f with increasing p mainly arises from an increased δR_p, as shown in Fig. 6(a) where the p dependence of δR_p is plotted for $Z=10$, 20, and 50 of a given ring with $N=100$. With increasing p, δR_p is linearly increased as $\delta R \propto p/Z$ for a small p. Figure 6(b) will be explained in Sec. IV.

Figure 7(a) shows the p dependence of $\gamma_{1,1}$, $\zeta_{1,1}$, and $\rho_{1,1}$ at the firing time with $J=0.02$, $\beta=0.005$, $N=100$, and $Z=10$; filled and open marks express results of DMA and direct simulations, respectively. At $p=0.0$, $\gamma_{1,1}$, $\zeta_{1,1}$, and $\rho_{1,1}$ are 0.671×10^{-3}, 0.131×10^{-3}, and 0.239×10^{-4}, respectively. In contrast, at $p=1.0$, they are 0.109×10^{-2}, 0.144×10^{-3}, and 0.232×10^{-4}, respectively. With increasing p, $\gamma_{1,1}$ is increased, while $\rho_{1,1}$ and $\zeta_{1,1}$ are almost constant. The difference between the p dependences of $\gamma_{1,1}$, $\rho_{1,1}$, and

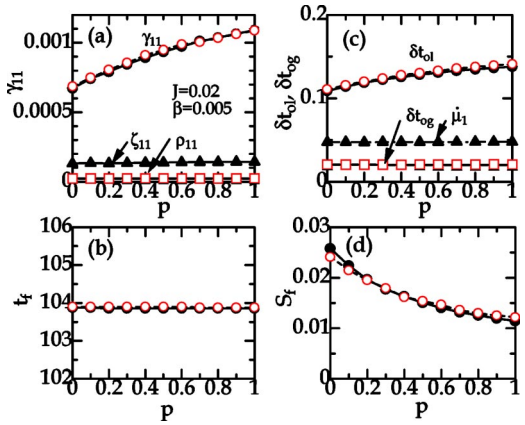

FIG. 7. (Color online) The p dependence of (a) the correlations of $\gamma_{1,1}$ (circles), $\zeta_{1,1}$ (triangles), and $\rho_{1,1}$ (squares) at the firing time, (b) the firing times t_f, (c) the firing-time accuracy of $\delta t_{o\ell}$ (circles), δt_{og} (squares), and $\dot{\mu}_1$ (triangles), and (d) the synchronization ratio at the firing time, S_f, for $\beta=0.005$, $J=0.02$, $N=100$, and $Z=10$: filled and open marks denote results of DMA and direct simulations, respectively. Results of $\zeta_{1,1}$ and $\dot{\mu}_1$ are only for DMA.

$\zeta_{1,1}$ arises from the fact that $d\gamma_{1,1}/dt$ in Eq. (23) has a contribution from ϕ_1 while $d\rho_{1,1}/dt$ and $d\zeta_{1,1}/dt$ in Eqs. (26) and (29) have no direct contributions from it. Figure 7(b) shows that the firing time of $t_f=103.88$ is independent of p, which is in accordance with a constant $\dot{\mu}_1$ shown in Fig. 7(c). Figure 7(c) shows that with increasing p, the firing-time accuracy of $\delta t_{o\ell}$ becomes worse because of an increased $\gamma_{1,1}$ while that of δt_{og} is independent of p. The p dependence of S_f is depicted in Fig. 7(d), which shows that the synchrony is decreased with increasing p. This clearly explains results of smaller S_f for larger p, having been shown in Figs. 5(a)–5(f).

IV. CONCLUSION AND DISCUSSION

Generalizing a phenomenological analysis adopted in I [24] based on calculated results of DMA, we have tried to get an analytical expression for S_f. From calculated results discussed in the previous section, we expand $\gamma_{1,1}$ and $\rho_{1,1}$ in a series of JZ and p:

$$\gamma_{1,1} = \gamma_0[1 - a_1 JZ(1 - a_2 p) + \cdots], \tag{53}$$

$$\rho_{1,1} = \frac{\gamma_0}{N}(1 + b_1 JZ + \cdots), \tag{54}$$

where $\gamma_o \propto \beta^2$, and a_1, a_2, and b_1 are positive coefficients. We have obtained an expression for $\gamma_{1,1}$ given by Eqs. (53), because the effect of p should vanish for $J=0$ or $Z=0$. Substituting Eqs. (53) and (54) into Eq. (52), we get

$$S_f = \left(\frac{[a_1(1 - a_2 p) + b_1]}{N - 1}\right) JZ + \cdots. \tag{55}$$

The expression for S_f given by Eq. (55) well explains the behavior shown in Figs. 4(d) and 7(d). Dependences of the quantities on N, Z, J, and β for local regular couplings are the same as those for all-to-all couplings having discussed in I. Typical examples of N dependence of various quantities are shown in Figs. 8(a)–8(d). Figures 8(a) and 8(b) show that $\rho_{1,1} \propto N^{-1}$ while $\gamma_{1,1}$, $\zeta_{1,1}$ and t_f are independent of N, which yields $\delta t_{0g} \propto N^{-1/2}$ and $\delta t_{0\ell} \propto N^0$, as shown in Fig. 8(c). Figure 8(d) shows that $S_f \propto N^{-1}$ both for local and global couplings, expressing that the synchronization is more easily realized in smaller networks than in larger ones.

In an early stage of this study, we obtained DE's given by Eqs. (21)–(34) with $\phi_1=\phi_2=0$, but with C and R which are replaced by C_p and R_p, respectively, given by [for details see after Eq. (A22) in the Appendix]

$$C_p = \left\langle \frac{1}{NZ^2} \sum_i \sum_j \sum_k c_{ij} c_{jk} c_{ik} \right\rangle_c, \tag{56}$$

$$R_p = \left\langle \frac{1}{NZ^2} \sum_i \sum_j \sum_k c_{ij} c_{jk} \right\rangle_c. \tag{57}$$

In this formulation, the effect of the coupling heterogeneity is included in the p-dependent clustering coefficient C_p and coupling connectivity R_p. The clustering coefficient C_p denotes an averaged fraction for given three nodes to be mutually coupled [13,14]. The p dependence of C_p is depicted in

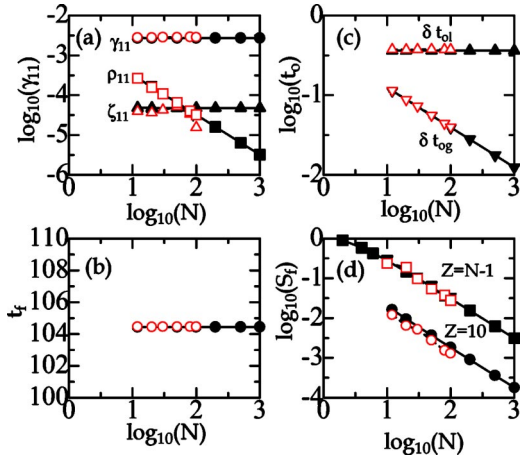

FIG. 8. (Color online) The N dependence of (a) the correlations of $\gamma_{1,1}$ (circles), $\zeta_{1,1}$ (triangles), and $\rho_{1,1}$ (squares) at the firing time, (b) the firing times t_f, (c) the firing-time accuracy of $\delta t_{o\ell}$ (circles) and δt_{og} (squares), and (d) the synchronization ratio at the firing time S_f ($\beta=0.01$, $J=0.002$, $p=0$, $N=100$, and $Z=10$): filled and open marks denote results of DMA and direct simulations, respectively. In (d) results for global couplings ($Z=N-1$) are also shown.

Fig. 6(b) which shows that with increasing p, C_p is decreased and approaches $C_p=Z/N$ at $p=1$. In contrast, the coupling connectivity R_p expresses an averaged fraction for given two nodes, which are not necessarily coupled, to have a common neighboring node. R_p in Eq. (57) may be rewritten as

$$R_p = \frac{1}{Z^2}\sum_K K^2 P(K) \equiv \frac{1}{Z^2}\overline{K^2}, \tag{58}$$

where the overline denotes the average over $P(K)$ expressing the probability for a given neuron to have K couplings [31]. It is easy to see that R_p is given by $R_p=1+\delta R_p$ [Eqs. (60) and (61)], the p dependence of δR_p being plotted in Fig. 6(a). Unfortunately, results calculated with the use of C_p and R_p for finite p were not in good agreement with those of direct simulations because effects of coupling heterogeneity are not properly taken into account in such DE's.

After several tries, we have obtained DE's having been given by Eqs. (21)–(36). C, R, and δC_p given by Eqs. (38)–(40) may be expressed in terms of C_p and R_p as [31]

$$C = C_0, \tag{59}$$

$$R = R_0 = 1, \tag{60}$$

$$\delta R_p = R_p - R_0 = \frac{1}{Z^2}\overline{(K-\overline{K})^2}, \tag{61}$$

with $Z=\overline{K}$. Figure 9 shows $P(K)$ for $p=0.0$, 0.1, 0.2, and 1.0 with $N=100$ and $Z=10$. In the limit of $p=0$, $P(K)(=\delta_{K,Z})$ is the delta function. With increasing p, $P(K)$ has the distribution centered at $K=Z$. In the limit of $p=1$, $P(K)$ approaches the Poisson distribution [16]. Figure 6(a) shows that with increasing p, δR_p is increased, while C_p is decreased as shown in Fig. 6(b). An increased δR_p yields an increase in $\gamma_{1,1}$, by which S_f is decreased and $\delta t_{o\ell}$ is increased. It should

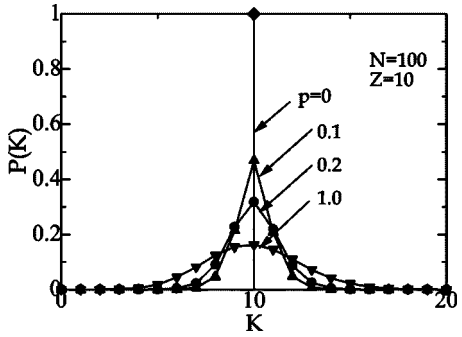

FIG. 9. The probability $P(K)$ for a given neuron to have K couplings for $p=0.0$, 0.1, 0.2, and 1.0 with $N=100$ and $Z=10$ in a SW ring.

be noted that effects of heterogeneous couplings are taken into account by δR_p through the correlation functions ϕ_1 and ϕ_2 in Eqs. (35) and (36), which play important roles in dynamics of SW networks.

To summarize, we have developed a semianalytical theory for SW networks of spiking FN neurons, including three kinds of spatial correlations: correlations of on-site, a coupled pair, and an uncoupled pair. By changing Z and p, we have performed model calculations of the response of the network to an external single spike. It has been shown that (i) when Z is increased, the synchronization ratio S_f and the firing-time accuracy $\delta t_{o\ell}$ are improved [Figs. 4(c) and 4(d)], which arises from a decrease in $\gamma_{1,1}$ and an increase in $\rho_{1,1}$, and (ii) when p is increased, both S_f and $\delta t_{o\ell}$ become worse [Figs. 7(c) and 7(d)] due to an increase in $\gamma_{1,1}$ induced by fluctuations in the coupling heterogeneity.

Item (i) is easily understood. The result for S_f in item (ii) is consistent with that of Ref. [20]. It, however, contradicts some calculations [17–19,21–23], which have claimed that the synchronization in SW networks is better than that in regular networks, since communication between neurons is more efficient because of the shorter characteristic path length L (as for the p dependence of L, see Fig. 2 of Ref. [13]). Our semianalytical theory with the use of the DMA, which is valid for weak noise ($\beta \ll 1$) and small coupling heterogeneity ($\delta R_p \ll 1$), has shown that the synchrony of SW networks depends on R, C, and δR_p given by Eqs. (38)–(40), but it is not affected by the average path length L. In particular, δR_p, ϕ_1, and ϕ_2 have been shown to play crucial roles in the dynamics of SW neural networks. Although item (ii) discussed above relies on the definition of the synchronization ratio of $S(t)$ given by Eq. (52), this conclusion is not changed even if we adopt an alternative measure for the synchrony. For example, when we employ R_s given by Eq. (49), R_s is increased with increasing p because of an increased $\gamma_{1,1}$, which again signifies the worse synchronization in SW networks. The semianalytical theory developed in this paper can be applied not only to SW neural networks but also to a wide class of complex SW networks. When we apply our theory to a general SW network in which the dynamics of each node is described by M-dimensional stochastic DE's, we get N_{eq}-dimensional deterministic DE's where $N_{eq}=M(3M+7)/2$. For example, $N_{eq}=5$ for Langevin model ($M=1$), $N_{eq}=13$ for FN model ($M=2$), and $N_{eq}=38$ for HH

model ($M=4$). Items (i) and (ii) [and also Eq. (55)] which have been derived for FN neuron model, are expected to hold for any SW network.

The present approach shares in its advantages with the original DMA previously proposed in I: (1) some results may be derived without numerical calculations because of its semianalytical nature, and (2) a computational time for a large-scale system by DMA is much shorter than that by direct simulations. By extending the ring geometry adopted in this paper, we may discuss the response of more realistic synfire-chain-type SW networks [24,32]. In the present paper, we have neglected the transmission time delay. Because the average path length L becomes shorter by the appearance of shortcuts [13–16], the response speed is expected to be improved in SW networks with time delays. Recently, we successfully applied the DMA to stochastic ensembles with time-delayed regular couplings [33,34]. By using our approach, we may discuss dynamics of general SW networks with time delays within the framework of the DMA. In the so-called *scale-free* (SF) networks such as the World Wide Web and the network of citations of scientific papers, the link connectivity $P(K)$ for a node to interact to K other nodes follows a power-law distribution $P(K)\sim K^{-\gamma}$ with the index γ ($\sim 2.1-4$) [35], in contrast to an exponential distribution for a large K in our SW networks (Fig. 9). This SF distribution probability originates from the two factors, the growth of nodes and their preferential attachment [35]. Quite recently it has been reported that the functional connectivity $P(K)$ versus the distance K in human brain is given by a SF distribution: $P(K)\sim K^{-2}$ [36]. It is interesting to apply our semianalytical approach to such SF networks. These subjects raised above are left to our future study.

ACKNOWLEDGMENT

This work was partly supported by a Grant-in-Aid for Scientific Research from the Japanese Ministry of Education, Culture, Sports, Science, and Technology.

APPENDIX: DERIVATION OF EQS. (21)–(36)

Substituting Eqs. (9) and (13) into Eqs. (1)–(4), we get DE's for δx_{1i} and δx_{2i} of a neuron i, given by (argument t is suppressed)

$$\frac{d\delta x_{1i}}{dt} = f_1\delta x_{1i} + f_2(\delta x_{1i}^2 - \gamma_{1,1}) + f_3\delta x_{1i}^3 - c\,\delta x_{2i} + \delta I_i^{(c)} + \xi_j, \tag{A1}$$

$$\frac{d\delta x_{2j}}{dt} = b\,\delta x_{1j} - d\,\delta x_{2j}, \tag{A2}$$

with

$$\delta I_i^{(c)}(t) = J\sum_j [g_1(t)c_{0ij}\delta x_{1j}(t) + g_0(t)\delta c_{ij} + g_1(t)\delta c_{ij}\delta x_{1j}(t) + \cdot], \tag{A3}$$

where $f_\ell = (1/\ell!)F^{(\ell)}$ and $g_\ell = (1/\ell!)G^{(\ell)}$. DE's for the correlations are given by

$$\frac{d\gamma_{\kappa,\lambda}}{dt} = \left\langle \frac{1}{N}\sum_i \left\langle \left[\delta x_{\kappa i}\left(\frac{d\delta x_{\lambda i}}{dt}\right) + \left(\frac{d\delta x_{\kappa i}}{dt}\right)\delta x_{\lambda i}\right]\right\rangle\right\rangle_c, \tag{A4}$$

$$\frac{d\zeta_{\kappa,\lambda}}{dt} = \left\langle \frac{1}{NZ}\sum_i\sum_j c_{ij}\left\langle \left[\delta x_{\kappa i}\left(\frac{d\delta x_{\lambda j}}{dt}\right) + \left(\frac{d\delta x_{\kappa j}}{dt}\right)\delta x_{\lambda i}\right]\right\rangle\right\rangle_c, \tag{A5}$$

$$\frac{d\rho_{\kappa,\lambda}}{dt} = \left\langle \frac{1}{N^2}\sum_i\sum_j \left\langle \left[\delta x_{\kappa i}\left(\frac{d\delta x_{\lambda j}}{dt}\right) + \left(\frac{d\delta x_{\kappa j}}{dt}\right)\delta x_{\lambda i}\right]\right\rangle\right\rangle_c. \tag{A6}$$

With the use of Eqs. (A1)–(A3), we may calculate DE's given by Eqs. (21)–(34). For example, terms including $\delta I_i^{(e)}$ in $d\gamma_{1,1}/dt$, $d\zeta_{1,1}/dt$, and $d\rho_{1,1}/dt$ become

$$\left\langle \frac{2}{N}\sum_i \langle \delta x_{1i}\delta I_i^{(c)}\rangle \right\rangle_c = \frac{2J}{N}\sum_i\sum_j g_1 c_{0ij}\langle\langle \delta x_{1i}\delta x_{1j}\rangle\rangle_c + \frac{2J}{N}\sum_i\sum_j g_0\langle\langle \delta x_{1i}\delta c_{ij}\rangle\rangle_c, \tag{A7}$$

$$= 2JZ[g_1\zeta_{1,1} + g_0\phi_1], \tag{A8}$$

$$\left\langle \frac{2}{NZ}\sum_i\sum_j c_{ij}\langle \delta x_{1i}\delta I_j^{(c)}\rangle \right\rangle_c = \frac{2J}{NZ}\sum_i\sum_j\sum_k g_1 c_{0ij}c_{0jk}\langle\langle \delta x_{1i}\delta x_{1k}\rangle\rangle_c + \frac{2J}{NZ}\sum_i\sum_j\sum_k g_0 c_{0ij}\langle\langle \delta x_{1i}\delta c_{jk}\rangle\rangle_c, \tag{A9}$$

$$= 2Jg_1[\gamma_{1,1} + ZC\zeta_{1,1} + (ZR - ZC - 1)\eta_{1,1}], \tag{A10}$$

$$\left\langle \frac{2}{N^2}\sum_i\sum_j \langle \delta x_{1i}\delta I_j^{(c)}\rangle \right\rangle_c = \frac{2J}{N^2}\sum_i\sum_j\sum_k g_1 c_{0jk}\langle\langle \delta x_{1i}\delta x_{1k}\rangle\rangle_c + \frac{2J}{N^2}\sum_i\sum_j\sum_k g_0\langle\langle \delta x_{1i}\delta c_{jk}\rangle\rangle_c, \tag{A11}$$

$$= \frac{2JZg_1}{N}[\gamma_{1,1} + ZR\zeta_{1,1} + (N - ZR - 1)\eta_{1,1}], \tag{A12}$$

where ϕ_κ ($\kappa=1,2$) are new correlation functions defined by

$$\phi_\kappa(t) = \left\langle \frac{1}{NZ}\sum_i\sum_j \langle \delta x_{\kappa i}(t)\delta c_{ij}\rangle \right\rangle_c, \quad \kappa = 1,2. \tag{A13}$$

In evaluating Eqs. (A7)–(A12), we have employed the relations given by

$$1 = \frac{1}{NZ}\sum_i\sum_j c_{0ij}, \tag{A14}$$

$$R = \frac{1}{NZ^2}\sum_i \sum_j \sum_k c_{0ij}c_{0jk}, \tag{A15}$$

$$C = \frac{1}{NZ^2}\sum_i \sum_j \sum_k c_{0ij}c_{0jk}c_{0ik}, \tag{A16}$$

$$\delta R_p = \frac{1}{NZ^2}\left\langle \sum_i \sum_j \sum_k \delta c_{ij}\delta c_{jk} \right\rangle_c, \tag{A17}$$

and the mean-field approximation given by

$$\langle\langle \delta x_{\kappa i}\delta x_{\lambda j}\rangle\rangle_c = \gamma_{\kappa,\lambda}\delta_{ij} + (1-\delta_{ij})[\zeta_{\kappa,\lambda}\delta_{ij}c_{ij} + \eta_{\kappa,\lambda}\delta_{ij}(1-c_{ij})], \tag{A18}$$

$$= \gamma_{\kappa,\lambda}\delta_{ij} + \zeta_{\kappa,\lambda}c_{ij} + \eta_{\kappa,\lambda}(1-\delta_{ij}-c_{ij}), \tag{A19}$$

$$\langle\langle \delta x_{\kappa,i}\delta c_{jk}\rangle\rangle_c = \phi_\kappa c_{jk}(\delta_{ij}+\delta_{ik}), \tag{A20}$$

with the Gaussian decoupling approximations [24]. In Eqs. (A18) and (A19), $\gamma_{\kappa,\lambda}$, $\zeta_{\kappa,\lambda}$, and $\eta_{\kappa,\lambda}$ denote the correlations of on-site, a coupled pair and an uncoupled pair, which are defined by Eqs. (12)–(16). The approximations given by Eqs. (A18)–(A20) are consistent with the definition of $\gamma_{\kappa,\lambda}$, $\zeta_{\kappa,\lambda}$, and $\eta_{\kappa,\lambda}$ given by Eqs. (14)–(16), and those of ϕ_κ given by Eq. (37).

The equations of motion of ϕ_κ are similarly calculated with the use of the relation given by

$$\frac{d\phi_\kappa}{dt} = \left\langle \frac{1}{NZ}\sum_i \sum_j \left\langle \left(\frac{d\delta x_{\kappa i}}{dt}\right)\delta c_{ij} \right\rangle \right\rangle_c, \tag{A21}$$

which yield Eqs. (35) and (36).

We have taken into account terms up to orders of $O((\delta x)^2)$, $O((\delta c/Z)^2)$, and $O(\delta x \delta c/Z)$ in Eqs. (21)–(36), and up to the order of $O((\delta x)^4)$ in the term including $a(=f_1+3f_3\gamma_{1,1})$ which plays an important role in stabilizing DE's [24].

On the contrary, when we adopt an expression given by

$$\delta I_i^{(c)}(t) = J\sum_j [g_1(t)c_{ij}\delta x_{1j}(t) + \cdot], \tag{A22}$$

instead of Eq. (A3), DE's given by Eqs. (A7), (A9), and (A11) become

$$\left\langle \frac{2}{N}\sum_i \langle \delta x_{1i}\delta I_i^{(c)}\rangle \right\rangle_c \simeq \frac{2J}{N}\sum_i \sum_j g_1\langle c_{ij}\langle\langle \delta x_{1i}\delta x_{1j}\rangle\rangle_c\rangle_c, \tag{A23}$$

$$= 2JZg_1\zeta_{1,1}, \tag{A24}$$

$$\left\langle \frac{2}{NZ}\sum_i \sum_j c_{ij}\langle \delta x_{1i}\delta I_j^{(c)}\rangle \right\rangle_c \simeq \frac{2J}{NZ}\sum_i \sum_j \sum_k g_1\langle c_{ij}c_{jk}\langle\langle \delta x_{1i}\delta x_{1k}\rangle\rangle_c\rangle_c, \tag{A25}$$

$$= 2Jg_1[\gamma_{1,1} + ZC_p\zeta_{1,1} + (ZR_p - ZC_p - 1)\eta_{1,1}], \tag{A26}$$

$$\left\langle \frac{2}{N^2}\sum_i \sum_j \langle \delta x_{1i}\delta I_j^{(c)}\rangle \right\rangle_c \simeq \frac{2J}{N^2}\sum_i \sum_j \sum_k g_1\langle c_{jk}\langle\langle \delta x_{1i}\delta x_{1k}\rangle\rangle_c\rangle_c, \tag{A27}$$

$$= \frac{2JZg_1}{N}[\gamma_{1,1} + ZR_p\zeta_{1,1} + (N - ZR_p - 1)\eta_{1,1}], \tag{A28}$$

where decoupling approximations such as

$$\langle c_{ij}\langle \delta x_{1i}\delta x_{1j}\rangle\rangle_c \simeq \langle c_{ij}\langle\langle \delta x_{1i}\delta x_{1j}\rangle\rangle_c\rangle_c \tag{A29}$$

and Eq. (A19) are employed. C_p and R_p in Eqs. (A26) and (A28) are given by Eqs. (56) and (57). Note that c_{ij} in Eqs. (A23), (A25), and (A27) depends on the configuration of couplings while c_{0ij} in Eqs. (A7), (A9), and (A11) does not. Then we got equations of motions given by Eqs. (21)–(34) with $\phi_1=\phi_2=0$ but with C and R which are, respectively, replaced by p dependent C_p and R_p given by Eqs. (56) and (57). As mentioned in Sec. IV, results calculated with the use of such DE's are not in good agreement with those obtained by direct simulations because effects of coupling fluctuations are not properly included in the formulation mentioned above. It is indispensable to take into account effects of the coupling heterogeneity expressed by δR_p through the correlation functions ϕ_1 and ϕ_2, as given by Eqs. (35) and (36).

[1] A. L. Hodgkin and A. F. Huxley, J. Physiol. (London) **117**, 500 (1952).

[2] R. FitzHugh, Biophys. J. **1**, 445 (1961).

[3] J. Nagumo, S. Arimoto, and S. Yoshizawa, Proc. IRE **50**, 2061 (1962).

[4] J. L. Hindmarsh and R. M. Rose, Nature (London) **296**, 162 (1982).

[5] H. Risken, *The Fokker-Planck Equation: Methods of Solution and Applications*, Springer Series in Synergetics, No. 18 (Springer-Verlag, Berlin, 1992).

[6] B. W. Knight, J. Gen. Physiol. **59**, 734 (1972); Neural Comput. **12**, 473 (2000); B. W. Knight, A. Omurtag, and L. Sirovich, Neural Comput. **12**, 1045 (2000); A. Omurtag, B. W. Knight, and L. Sirovich, J. Comput. Neurosci. **8**, 51 (2000).

[7] D. Q. Nykamp and D. Tranchina, J. Comput. Neurosci. **8**, 19 (2000); E. Haskell, D. Q. Nykamp, and D. Tranchina, Network **12**, 141 (2000).

[8] R. Rodriguez and H. C. Tuckwell, Phys. Rev. E **54**, 5585 (1996).

[9] H. C. Tuckwell and R. Rodriguez, J. Comput. Neurosci. **5**, 91

(1998).
[10] R. Rodriguez and H. C. Tuckwell, BioSystems **48**, 187 (1998).
[11] R. Rodriguez and H. C. Tuckwell, Math. Comput. Modell. **31**, 175 (2000).
[12] N. Fourcaud and N. Brunel, Neural Comput. **14**, 2057 (2002).
[13] D. J. Watts and S. H. Strogatz, Nature (London) **393**, 440 (1998).
[14] S. H. Strogatz, Nature (London) **410**, 268 (2001).
[15] M. E. J. Newman, J. Stat. Phys. **101**, 819 (2000).
[16] R. Albert and A. Barabasi, Rev. Mod. Phys. **74**, 47 (2002).
[17] L. F. Lago-Fernández, R. Huerta, F. Corbacho, and J. A. Sigüenza, Phys. Rev. Lett. **84**, 2758 (2000).
[18] M. Barahona and L. M. Pecora, Phys. Rev. Lett. **89**, 054101 (2002).
[19] M. Bucolo, L. Fortuna, and M. La Rosa, Chaos, Solitons Fractals **14**, 1059 (2002).
[20] T. Nishikawa, A. E. Motter, Y. Lai, and F. C. Hoppensteadt, Phys. Rev. Lett. **91**, 014101 (2003).
[21] O. Kwon and H. Moon, Phys. Lett. A **298**, 319 (2002).
[22] H. Hong, M. Y. Choi, and B. J. Kim, Phys. Rev. E **65**, 026139 (2002).
[23] H. Hong, M. Y. Choi, and B. J. Kim, Phys. Rev. E **65**, 047104 (2002).
[24] H. Hasegawa, Phys. Rev. E **67**, 041903 (2003).
[25] H. Hasegawa, Phys. Rev. E **68**, 041909 (2003).
[26] When the DMA is applied to N-unit neuron networks with global, regular couplings, in which dynamics of each neuron is described by M variables, MN-dimensional stochastic DE's are replaced by N_{eq}-dimensional deterministic DE's where $N_{eq}=M(M+2)$ [25]. In contrast, when the moment method [8] is employed, we get $N_{eq}=(1/2)MN(MN+3)$. In the case of $N=1000$, for example, we get $N_{eq}=8(2003\,000)$ for $M=2$, and $24(8006\,000)$ for $M=4$ in the DMA (the moment method).
[27] S. Tanabe and K. Pakdaman, Phys. Rev. E **63**, 031911 (2001).
[28] S. Tanabe, S. Sato, and K. Pakdaman, Phys. Rev. E **60**, 7235 (1999).
[29] S. Tanabe and K. Pakdaman, Biol. Cybern. **85**, 269 (2001).
[30] The normalization factor in front of the coupling term is N^{-1} in I while it is unity in this paper; results of the former are obtainable from the latter by a replacement of $J \to w/N$.
[31] We may show that $Z=\langle(1/N)\Sigma_{ij}c_{ij}\rangle_c=\Sigma_K KP(K)$ and $R_p=\langle(1/NZ^2)\Sigma_{ijk}c_{ij}c_{jk}\rangle_c=Z^{-2}\Sigma_K K^2P(K)$, by defining the probability: $P(K)=\langle(1/N)\Sigma_i\delta(K-\Sigma_j c_{ij})\rangle_c$. This implies that $\delta R_p=R_p-R_0=Z^{-2}\Sigma_K K^2[P(K)-P_0(K)]=Z^{-2}\Sigma_K K^2P(K)-1=Z^{-2}\Sigma_K(K-Z)^2P(K)$ which leads to Eq. (61), $P_0(K)(=\delta_{K,Z})$ denoting the probability for $p=0$.
[32] M. Abeles, H. Bergman, E. Margalit, and E. Vaadia, J. Neurophysiol. **70**, 1629 (1993).
[33] H. Hasegawa, Phys. Rev. E **70**, 021911 (2004).
[34] H. Hasegawa, Phys. Rev. E **70**, 021912 (2004).
[35] A. Barabási and R. Albert, Nature (London) **286**, 509 (1999).
[36] D. R. Chialvo, Physica A **340**, 756 (2004).